Aggregation of β-amyloid fragments

Jan H. Meinke, and Ulrich H. E. Hansmann

Citation: The Journal of Chemical Physics **126**, 014706 (2007); doi: 10.1063/1.2423013
View online: https://doi.org/10.1063/1.2423013
View Table of Contents: http://aip.scitation.org/toc/jcp/126/1
Published by the American Institute of Physics

Aggregation of β-amyloid fragments

Jan H. Meinke[a)]
John-von-Neumann Institute for Computing, Forschungszentrum Jülich, D-52425 Jülich, Germany

Ulrich H. E. Hansmann[b)]
John-von-Neumann Institute for Computing, Forschungszentrum Jülich, D-52425 Jülich, Germany and Department of Physics, Michigan Technological University, Houghton, Michigan 49931

(Received 26 September 2006; accepted 21 November 2006; published online 4 January 2007)

The authors study the folding and aggregation of six chains of the β-amyloid fragment 16–22 using Monte Carlo simulations. While the isolated fragment prefers a helical form at room temperature, in the system of six interacting fragments one observes both parallel and antiparallel β sheets below a crossover temperature $T_x \approx 420$ K. The antiparallel sheets have lower energy and are therefore more stable. Above the nucleation temperature the aggregate quickly dissolves into widely separated, weakly interacting chains. © *2007 American Institute of Physics*.
[DOI: 10.1063/1.2423013]

I. INTRODUCTION

Isolated proteins fold into unique three-dimensional structures that are determined by their amino-acid sequence. In the cell, however, proteins are never isolated. Already during folding, proteins interact with the ribosomes and with each other. Chaperones, e.g., help proteins fold correctly. But the crowded environment can also lead to unwanted consequences. At least for some sequences it depends on the local environment whether they form α helices or β strands. In some cases, the presence of a β strand catalyzes the formation of a sheet even in sequences that otherwise form helices.[1,2] The newly folded sheet is often at the exterior, making such misfolded structures prone to aggregate and, as the catalytic process repeats, successively form fibrils. Such fibrils seem to be involved as a general mechanism in a number of diseases such as Alzheimer's, Huntington's, or spongiform encephalopathies (prion mediated).[3] The most common of these diseases is Alzheimer's. Associated with its neuropathology are amyloid deposits composed mainly of the β-amyloid peptide (Aβ). It is found in body fluids in a soluble form that has partial α-helical structure. In Alzheimer's disease, Aβ undergoes a conformational change toward a β-sheet structure in which it is insoluble and assembles into fibrils 60–90 Å in diameter. Fibrillar amyloids form lesions 10–200 μm in diameter, known as senile plaques. These plaques are surrounded by degenerating and swollen nerve terminals and are found in the extracellular space of the brain. The neurotoxicity of Aβ is related to the degree of β aggregation. Hence, an understanding of the aggregation mechanism could contribute to the developing understanding of the biogenesis of this devastating neurological disorder[3] and may lead to more targeted treatments.

Simulations are an important tool to research the mechanism of aggregation in the amyloid peptide[4–8] and other proteins. Even using all-atom models, such numerical investigations are possible because experimental evidence indicates that already several fragments of Alzheimer's β-amyloid can form fibrils. Some authors find evidence for the formation of parallel sheets in Aβ_{10-35} (Ref. 9) and Aβ_{1-40} (Ref. 10). Others have reported antiparallel strands, for example, in Aβ_{34-42},[11] Aβ_{11-25},[12] and Aβ_{16-22}.[13,14] Recently Lührs *et al.* looked at the aggregation of the whole Aβ_{1-42} protein. They found in NMR studies[15] that the residues 18–26 form a β sheet that is in registry with a β sheet formed by residues 31–42 of a second β-amyloid molecule. Almost all of these studies contain the fragment 16–22, which has already been identified as a key element in 1996 by Tjernberg *et al.*[16] Hence, a number of different computational studies have focused on this fragment. Gnanakaran *et al.*,[4] e.g., found multiple basins in the free energy landscape and concluded that Aβ_{16-22} can form other stable configurations aside from parallel and antiparallel sheets. Using molecular dynamics simulations, Klimov and Thirumalai[5] found that the formation of the aggregate requires an intermediate helical phase. They emphasize the distinct roles of the hydrophobic interactions, which provide the driving force for the initial collapse, and the electrostatic interaction, which result in the formation and stabilization of antiparallel β sheets. In fact they conclude that "the ordered (antiparallel) orientation is only obtained upon the formation of salt bridges." However, Favrin *et al.*[6] found antiparallel β sheets as the free energy minimum of their Monte Carlo simulation as well, despite the fact that they ignored interactions between side chain charges in their model.

In order to resolve this discrepancy and to test whether the results of Ref. 6 are artifacts of the specific protein model or universal, we have reproduced these simulations using the ECEPP/3 force field with an additional implicit solvent term and different end groups. Our simulation results show that the isolated fragment Aβ_{16-22} has a propensity to form α helices. However, in a crowded environment, it becomes

[a)]Electronic mail: j.meinke@fz-juelich.de
[b)]Electronic mail: u.hansmann@fz-juelich.de

TABLE I. Temperatures used for parallel tempering in K. The calculation for each replica was performed on a separate processor.

T_1	T_2	T_3	T_4	T_5	T_6	T_7	T_8	T_9	T_{10}	T_{11}	T_{12}
250	267	284	300	325	345	266	380	393	400	408	411
T_{13}	T_{14}	T_{15}	T_{16}	T_{17}	T_{18}	T_{19}	T_{20}	T_{21}	T_{22}	T_{23}	T_{24}
415	418	421	423	425	430	435	437	440	442	446	450
T_{25}	T_{26}	T_{27}	T_{28}	T_{29}	T_{30}	T_{31}	T_{32}				
456	460	466	475	500	550	600	700				

energetically favorable to form strands, and both parallel and antiparallel β sheets are observed by us, with the antiparallel form being more stable due to energetically favored side chain arrangement.

II. METHODS

In order to study aggregation of the seven-residue fragment β-amyloid$_{16-22}$ we perform a parallel tempering simulation of a system of six interacting molecules. In contrast to Ref. 6 we use NH_2 (instead of an N-acetyl group) as N-terminal end group and COOH (instead of NH_2) as C-terminal end group. Each configuration of the system is characterized by an energy E_{tot} that is the sum of three terms,

$$E_{\text{tot}} = E_{\text{ECEPP/3}} + E_{\text{imol}} + E_{\text{solv}}. \tag{1}$$

The intramolecular interactions are described by the ECEPP/3 force field[17] and given as the sum of electrostatic energy E_C, Lennard-Jones term E_{LJ}, hydrogen-bond energy E_{hb}, and torsion energy E_{tor},

$$\begin{aligned} E_{\text{ECEPP/3}} &= E_C + E_{\text{LJ}} + E_{\text{hb}} + E_{\text{tor}} \\ &= \sum_{(i,j)} \frac{332 q_i q_j}{\epsilon r_{ij}} + \sum_{(i,j)} \left(\frac{A_{ij}}{r_{ij}^{12}} - \frac{B_{ij}}{r_{ij}^{6}} \right) \\ &\quad + \sum_{(i,j)} \left(\frac{C_{ij}}{r_{ij}^{12}} - \frac{D_{ij}}{r_{ij}^{10}} \right) + \sum_{l} U_l (1 \pm \cos(n_l \xi_l)), \end{aligned} \tag{2}$$

where r_{ij} is the distance between the atoms i and j, ξ_l is the lth torsion angle, and energies are measured in kcal/mol. The intermolecular interaction E_{imol} includes hydrogen bonding E_{hb}, Lennard-Jones interactions E_{LJ}, and Coulomb interactions E_C. These energies are defined in the same way as for intramolecular terms but act only between atoms that belong to different fragments. The protein-solvent interactions are approximated by a solvent accessible surface term,

$$E_{\text{solv}} = \sum_i \sigma_i A_i. \tag{3}$$

Here A_i is the solvent accessible surface area of the ith atom in a given configuration, and σ_i is a solvation parameter for the atom i.[18] Our simulation relies on the implementation of these interactions in Version 3 of the program package SMMP,[19,20] the first version to support multimolecule simulations and described in detail in Ref. 21.

The above atomistic model contains both attractive and repulsive interactions. As a consequence, the resulting energy landscape is characterized by a multitude of local minima separated by high energy barriers. Hence, sampling of low-energy conformations is a hard computational task. Physical quantities cannot be calculated accurately from simple low-temperature molecular dynamics or Monte Carlo simulations. One way to overcome this so-called multiple-minima problem is parallel tempering[22,23] first used in protein science in Ref. 24. In this method, several replicas of the system are simulated in parallel at different temperatures. Configurations are exchanged between replicas every n_{ex} steps with probability

$$P(i \leftrightarrow j) = \min(1, \exp((\beta_i - \beta_j)(E_i - E_j))). \tag{4}$$

For the present simulation we used 32 replicas with temperatures from $T_{\text{min}}=250$ K to $T_{\text{max}}=700$ K, as listed in Table I. We use a 50 Å box with hard walls. This gives rise to a high density compared to the experiments and is necessary due to the much smaller number of chains in the simulation. An exchange was attempted every ten Monte Carlo sweeps. The simulation ran over 100 000 sweeps, where each sweep consists not only of a series of Metropolis updates of the internal angles in all chains but also of the rigid body coordinates of each molecule. The maximum step size along each axis is 0.5 Å, and the angles are changed randomly between $-\pi$ and π. The starting configurations were obtained from an initial equilibration run that also served to adjust the temperatures of the replicas. For comparison, we also simulate with the same protocol and energy function a single seven-residue fragment β-amyloid$_{16-22}$.

III. SIMULATION RESULTS

We start by presenting our results for an isolated fragment β-amyloid$_{16-22}$. Figure 1 displays the secondary structure content as a function of temperature. We observe two distinct temperature regions. At high temperatures, the peptide is a random coil with low sheet and helical content, while at low temperatures helical configurations dominate. Here and in the following we define a residue as helical if its dihedral angle pair (ϕ, ψ) takes values of $(-70° \pm 30°, -37° \pm 30°)$. Similarly, we define a residue as sheetlike if this pair takes values of $(-150° \pm 30°, 150° \pm 30°)$. The helical propensity h is the average fraction of helical residues, and the sheet propensity s is the average fraction of sheetlike residues. The crossover between the two temperature regions occurs around $T \approx 325$ K where the specific heat has a corresponding peak (see the inset of Fig. 1). Hence, in our model at room temperature the isolated fragment has an in-

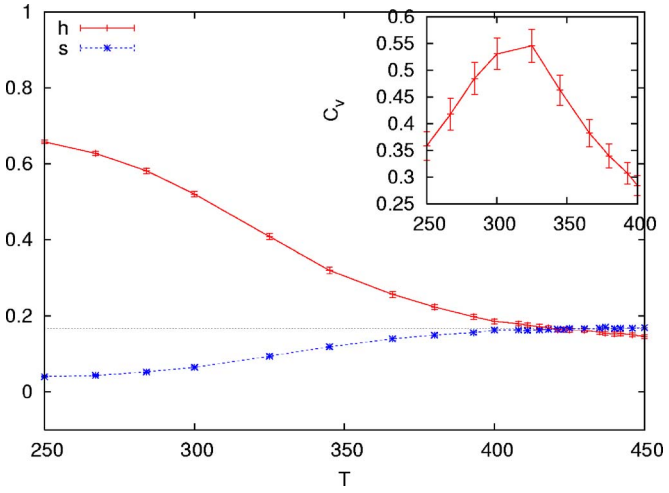

FIG. 1. (Color online) Secondary structure content for a single β-amyloid$_{16-22}$ fragment. At temperatures below 325 K, the helical content h (solid line) of the fragment dominates. It falls off to the value for a random coil at high temperatures. The sheet content s is suppressed below the random value at low temperatures. The high-temperature propensity values h and s for a random coil are indicated by the straight dotted line. Its value is not 1/36, as one might expect from the ϕ-ψ ranges of our defintion, but 1/6, indicating the approximate area of the allowed region in the corresponding Ramachadran plots. The inset shows the specific heat of the random coil-helix crossover of a single fragment. The significant change in the helix propensity coincides with the specific-heat peak at $T \approx 325$ K. Error bars in this and the following figures represent statistical errors and are often of the order of or smaller than the symbol size.

trinsic tendency to form helices. This result is in contrast to Ref. 6, where they report only an insignificant increase in the helix propensity at low temperatures, but not unreasonable. For various peptides (see, for instance, Ref. 25) it has been observed that such short sequences prefer to adapt a helical configuration when isolated, while they may take different shapes when interacting with other molecules. For the isolated fragment β-amyloid$_{16-22}$ the preference for forming helices is due to their lower energy. With our energy function, the minimum energy of an all-helical isolated fragment is −46.8 kcal/mol, but −34.43 kcal/mol for an all-strand isolated fragment. Hence, formation of a helical configuration is preferred by about 12 kcal/mol, an energy difference that results mostly from the Lennard-Jones term in the more densely packed helix and easily overcomes the increased solvation term. Table II lists all energy terms for both configurations.

The question of how the situation changes when we no longer have a single isolated molecule but a system of six interacting β-amyloid 16–22 fragments arises. In Fig. 2 we display the specific heat of this compound system. Again, one observes a peak in the specific heat, shifted now to a temperature $T \approx 420$ K, that separates a high-temperature phase from one at low temperatures. The corresponding plot

TABLE II. Partial energies for minimum energy single peptide helix and strand configuration. All energies are given in kcal/mol.

	E_C	E_{LJ}	E_{hb}	E_{tor}	E_{sol}	E_{tot}
Helix	28.24	−42.49	−7.86	2.96	−27.67	−46.83
Strand	30.36	−30.53	−3.16	1.26	−32.24	−34.30

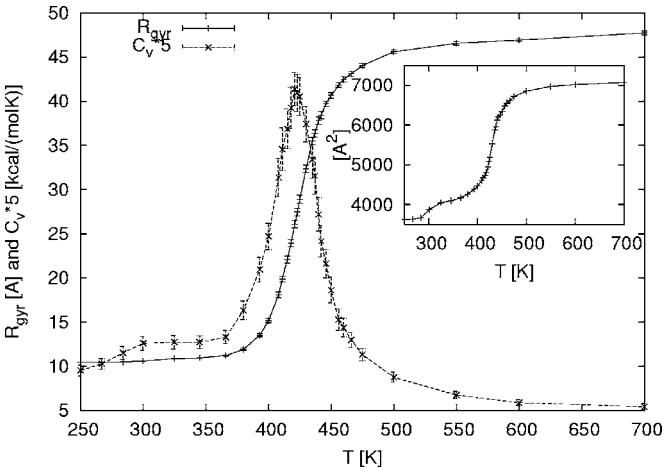

FIG. 2. Radius of gyration, specific heat, and accessible surface area vs temperature. A sharp crossover is evident around 425 K. The apparent saturation of R_{gyr} is an artifact of our fixed size bounding box. The crossover is mirrored by a corresponding crossover in the solvent accessible surface area (see inset). It also shows up as a peak in the specific heat C_v. The specific heat has been scaled up by a factor of five to emphasize the correspondence.

of the radius of gyration R_{gyr} (calculated over all atoms in the system) shows that this peak marks a sharp crossover from compact, aggregated structures at low temperatures to extended and isolated configurations at high temperatures T. Note that the apparent saturation of R_{gyr} is an artifact of our bounding box. The compactification happens despite an *increase* in the solvation energy with decreasing temperature that can be seen in the inset of Fig. 3. It is driven by a decrease in the interaction energy (shown also in Fig. 3) that is almost an order of magnitude larger than the increase in solvation energy. As a consequence, the total energy also decreases sharply with decreasing T, leading to the peak in specific heat observed in Fig. 2. The value of the crossover temperature $T \approx 420$ K is unphysiologically high. This is a problem with our energy function and has been observed in previous simulations.[26]

Typical snapshots of the system in these two phases are displayed in Fig. 4(a) (which shows a typical high-

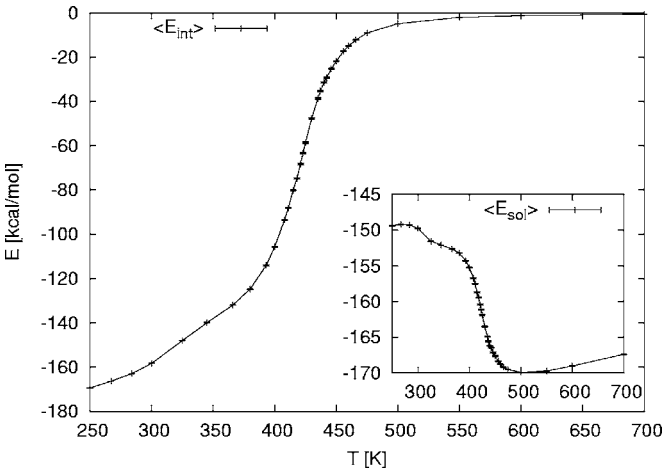

FIG. 3. Partial energies vs T. The decrease in the intermolecular interactions energy with decreasing temperature drives the aggregation despite an increase in the solvent energy term E_{sol} (inset). The intramolecular energy contributions do not show the crossover.

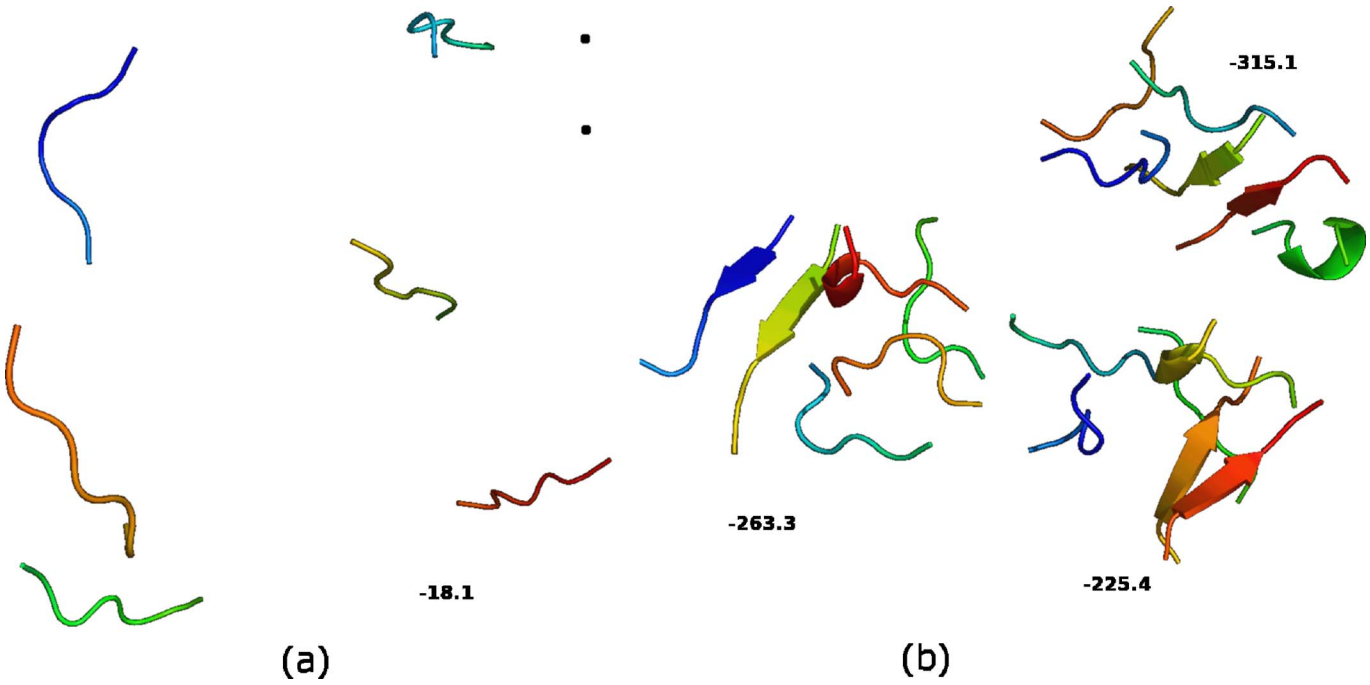

FIG. 4. (Color online) Sample configurations above and below the crossover. (a) Weakly interacting chains at $T > T_x$. (b) Aggregates at $T < T_x$.

temperature configuration of our system) and Fig. 4(b) (showing dominant low-temperature configurations). Consistent with the snapshots, we find in the high-temperature phase little secondary content (data not shown); below the crossover β sheets dominate. At room temperature, sheets appear with a frequency of 20%, while 15% of configurations are helical. With decreasing temperature, the importance of β strands becomes more and more pronounced. The substantial propensity of helical structures is consistent with the results by Klimov and Thirumalai[5] who also observed an intermediate helical phase.

As one can see from Fig. 4(b), β-amyloid$_{16-22}$ forms stable aggregates quickly in agreement with previous simulations. Note that antiparallel β sheets occur at lower energies than parallel ones. Here we consider a sheet parallel if there are at least three hydrogen bonds between the chains, at least 1/3 of the residues are sheetlike, and the scalar product of the end-to-end vectors of the strands is larger than 0.7. If the scalar product is instead less than −0.7, the sheet is antiparallel. Antiparallel β sheets appear to be not only energetically favored but also, at room temperature, observed with higher frequency albeit the free energy difference is only of order of k_BT.

Our result is in agreement with the previous work by Favrin *et al.* These authors report an increasing fraction of antiparallel sheets for larger systems and lower temperatures although their model does not include any Coulomb interaction. They argue that other effects, e.g., the arrangement of hydrophobic side chains or simple steric constraints, may prefer antiparallel alignment of sheets. This hypothesis is in contradiction to that of Klimov and Thirumalai[5] who emphasize that the antiparallel sheets are favored because of salt-bridge formation. Our results do not support Klimov and Thirumalai's hypothesis. We do not use charged residues in our simulations and therefore do not observe any salt bridges. We, nevertheless, find antiparallel β sheets energetically favored. The main contribution comes from the interaction *between* fragments by the Lennard-Jones term which favors the antiparallel configuration over parallel ones by 9.6 kcal/mol. This indicates a better packing of the side chains in the antiparallel configuration. Consequently, the solvent accessible surface area of hydrophobic residues is here 5% smaller than in the parallel configuration. Hence, our results support the findings of Favrin *et al.* that the formation of antiparallel β-sheet aggregates does not require formation of salt bridges but is due to optimized side chain packing in this configuration. A detailed study of the free energy landscape is left for future work.

IV. CONCLUSIONS

We have studied the folding and aggregation of six chains of the β-amyloid fragment 16–22. An isolated fragment prefers a helical form at room temperature. In the system of the six interacting fragments aggregates of parallel and antiparallel β sheets dominate below a crossover temperature $T_x \approx 420$ K. We find that antiparallel sheets are not stabilized by salt bridges but through energetically favored side chain arrangements.

ACKNOWLEDGMENTS

One of the authors (U.H.E.H.) acknowledges support by a research grant (Grant No. CHE-0313618) of the National Science Foundation (U.S.A.). The simulations were done on the Cray XD1 and the JUMP supercomputer of the John von Neumann Institute for Computing at the Research Center Jülich.

[1] Y. Peng and U. H. E. Hansmann, Biophys. J. **82**, 3269 (2002).
[2] Y. Peng, U. H. E. Hansmann, and N. A. Alves, J. Chem. Phys. **118**, 2374 (2003).
[3] J. C. Rochet and P. T. Lausbury, Jr., Curr. Opin. Struct. Biol. **10**, 60 (2000).
[4] S. Gnanakaran, R. Nussinov, and A. E. Garcia, J. Am. Chem. Soc. **128**, 2158 (2006).
[5] D. K. Klimov and D. Thirumalai, Structure (London) **11**, 295 (2003).
[6] G. Favrin, A. Irbäck, and S. Mohanty, Biophys. J. **87**, 3657 (2004).
[7] E. Malolepsza, M. Boniecki, A. Kolinski, and L. Piela, Proc. Natl. Acad. Sci. U.S.A. **102**, 7835 (2004).
[8] B. Tarus, J. Straub, and D. Thirumalai, J. Mol. Biol. **345**, 1141 (2005).
[9] T. S. Burkoth, T. L. S. Benzinger, V. Urban, D. M. Morgan, D. M. Gregory, P. Thiyagarajan, R. E. Botto, S. C. Meredith, and D. G. Lynn, J. Am. Chem. Soc. **122**, 7883 (2000).
[10] A. T. Petkova, Y. Ishii, J. J. Balbach, O. N. Antzutkin, R. D. Leapman, F. Delaglio, and R. Tycko, Proc. Natl. Acad. Sci. U.S.A. **99**, 16742 (2002).
[11] P. T. Lansbury, P. R. Costa, J. M. Griffiths *et al.*, Nat. Struct. Biol. **2**, 990 (1995).
[12] A. T. Petkova, G. Buntkowsky, F. Dyda, R. D. Leapman, W.-M. Yau, and R. Tycko, J. Mol. Biol. **335**, 247 (2004).
[13] J. Balbach, Y. Ishii, O. Antzutkin, R. Leapman, N. Rizzo, F. Dyda, J. Reed, and R. Tycko, Biochemistry **39**, 13748 (2000).
[14] D. Gordon, J. Balbach, R. Tycko, and S. Meredith, Biophys. J. **86**, 428 (2004).
[15] T. Lührs, C. Ritter, M. Adrian, D. Riek-Loher, B. Bohrmann, H. Doebeli, D. Schubert, and R. Riek, Proc. Natl. Acad. Sci. U.S.A. **102**, 17342 (2005).
[16] L. O. Tjernberg, J. Naslund, F. Lindqvist, J. Johansson, A. R. Karlstrom, J. Thyberg, L. Terenius, and C. Nordstedt, J. Biol. Chem. **271**, 8545 (1996).
[17] G. Nemethy, K. D. Gibson, K. A. Palmer, C. N. Yoon, G. Paterlini, A. Zagari, S. Rumsey, and H. A. Scheraga, J. Phys. Chem. **96**, 6472 (1992).
[18] T. Ooi, M. Oobatake, G. Nemethy, and H. A. Scheraga, Proc. Natl. Acad. Sci. U.S.A. **84**, 3086 (1987).
[19] F. Eisenmenger, U. H. E. Hansmann, S. Hayryan, and C.-K. Hu, Comput. Phys. Commun. **138**, 192 (2001).
[20] F. Eisenmenger, U. H. E. Hansmann, S. Hayryan, and C.-K. Hu, Comput. Phys. Commun. **174**, 422 (2006).
[21] J. H. Meinke and U. H. E. Hansmann, SMMP, http://www.fz-juelich.de/nic/cbb (2006).
[22] K. Hukushima and K. Nemoto, J. Phys. Soc. Jpn. **65**, 1604 (1996).
[23] C. J. Geyer and E. A. Thompson, J. Am. Stat. Assoc. **90**, 909 (1995).
[24] U. H. E. Hansmann, Chem. Phys. Lett. **281**, 140 (1997).
[25] Y. Peng and U. H. E. Hansmann, Phys. Rev. E **68**, 041911 (2003).
[26] C.-Y. Lin, C.-K. Hu, and U. H. E. Hansmann, Proteins: Struct., Funct., Genet. **52**, 436 (2003).